Xenon systematics of individual lunar zircons, a new window on the history of the lunar surface

Carolyn A. Crow [a,*], Sarah A. Crowther [b], Kevin D. McKeegan [c],
Grenville Turner [b], Henner Busemann [d], Jamie D. Gilmour [b]

[a] *Department of Geological Sciences, University of Colorado Boulder, United States*
[b] *School of Earth and Environmental Sciences, The University of Manchester, UK*
[c] *Department of Earth, Planetary, and Space Sciences, University of California, Los Angeles, United States*
[d] *ETH Zürich, Switzerland*

Abstract

We demonstrate a new way of investigating the processing of the lunar surface (and other planetary regoliths) that combines Xe_S-Xe_N ages (based on uranium fission) in individual zircons with their xenon isotopic record of solar wind and cosmic ray exposure. We report the first xenon isotopic analyses of individual lunar zircons (from Apollo 14 soil and breccias samples). Parallel analyses of a suite of zircons from the Vredefort impact structure in South Africa revealed Xe_S-Xe_N ages that agree well with U-Pb systematics, suggesting that the diffusion kinetics of xenon and lead in zircon are similar in the pressure-temperature environment of sub-basin floors. In contrast, all Apollo 14 zircons examined exhibit Xe_S-Xe_N ages markedly younger than the associated U-Pb and ^{207}Pb-^{206}Pb ages, and soil zircons with ^{207}Pb-^{206}Pb ages greater than 3900 Ma produced an abundance of Xe_S-Xe_N ages <1000 Ma. The young ages cannot be explained by thermal neutron irradiation on the lunar surface, and diurnal heating is unlikely to cause preferential loss of xenon. As such these young soil zircon ages likely record regolith gardening processes. The breccia zircons typically record older ages, >2400 Ma, suggesting that these samples may be useful for investigating ancient events and regolith processing at an earlier epoch. However, none of the zircons contain xenon from now-extinct ^{244}Pu implying that either the samples have completely degassed since ~3900 Ma or that the initial Pu/U ratio of the Moon is lower than that on Earth. We also describe a methodology for conducting component deconvolution that can be applied to multi-isotopes systems beyond xenon. We have also determined new xenon isotopic yields from rare earth element spallation in the lunar environment and high precision yields for neutron induced fission of ^{235}U in geologic samples.

© 2020 The Authors. Published by Elsevier Ltd. This is an open access article under the CC BY license (http://creativecommons.org/licenses/by/4.0/).

Keywords: Xenon; Zircon; Impact; Lunar; Regolith

1. INTRODUCTION

In the absence of a significant, persistent atmosphere and a magnetic field, the lunar surface is subject to bombardment by projectiles, high energy particles, and the solar wind (e.g. Podosek et al., 1971; Reedy and Arnold, 1972; Hörz et al., 1991). The samples returned by the Apollo missions provide one of the most accessible records of these processes, which are responsible for modifying surfaces of all airless bodies in our solar system. The majority of the Apollo samples at some level have experienced modification due to residence in the lunar regolith. This is evident in the abundance of breccia samples in the Apollo collection, as well as chemical

---

and isotopic variations resulting from processes such as vaporization and cosmic ray spallation (e.g. McKay et al., 1991). Although processes associated with regolith formation and evolution can create problems for determining endogenic geochemical and geochronologic information (e.g. Turner et al., 1971; Gaffney et al., 2011), regolith samples are useful for investigating the relative importance of impacts and exposure to cosmic rays, solar wind, and intense electromagnetic radiation in the evolution of planetary surfaces that are unprotected by atmospheres or magnetic fields. The xenon isotopic compositions of lunar zircons provide an useful system to probe the complicated history of regolith samples because the nine stable isotopes record time-sensitive information as well as signatures of cosmic ray spallation and exposure to the solar wind (Ozima and Podosek, 2001). Additionally, because zircons are robust crystals, many of which appear to have formed in the earliest periods of lunar volcanism, they potentially retain a record of billions of years of crustal evolution (e.g. Nemchin et al., 2008; Hopkins and Mojzsis, 2015; Crow et al., 2017). However, each zircon grain within the regolith is detrital and has an independent history, thus this record must be examined by analyzing a large suite of individual grains. Here, we validate the approach in a study of individual zircon grains from the Vredefort impact structure, which allows us to understand the response of this system to large-scale impact events. We then present the first xenon isotope study of individual lunar zircons and interpret the record they provide of the evolution of the lunar surface.

1.1. Overview of lunar zircons

One of the main advantages of the mineral zircon for deciphering complex histories is that multiple geochronometers with different closure temperatures can be investigated on individual mineral grains. The three main geochronological systems that have previously been applied to the lunar zircon population are U-Pb, U-Th-He, and Lu-Hf. The U-Pb and ^{207}Pb-^{206}Pb ages have been well characterized for zircons from all Apollo landing sites except Apollo 16 via secondary ion mass spectrometry (Meyer et al., 1996; Nemchin et al., 2006, 2008, 2009; Pidgeon et al., 2007; Taylor et al., 2009; Grange et al., 2013a, 2013b; Hopkins and Mojzsis, 2015; Crow et al., 2017), and there has been one study of Apollo 14 zircons by thermal ionization mass spectrometry (Barboni et al., 2017). The lunar zircons yielded crystallization ages ranging from 3942 ± 9 to 4417 ± 6 Ma (1σ) indicating that these grains are among the oldest dated materials from the Moon. The two studies that included zircons extracted from Apollo regolith, or soil, found that the ranges in ages of regolith grains reflect those of breccias from the same landing site (Taylor et al., 2009; Crow et al., 2017). The vast majority of zircons yield concordant U-Pb ages also suggesting that few grains have been exposed to prolonged high temperatures since crystallization (e.g. Crow et al., 2017). The Lu-Hf model ages from Taylor et al. (2009) and Barboni et al. (2017) further support the conclusion that the lunar zircons derive from an ancient crustal reservoir on the Moon, suggesting that the zircons crystallized

from a KREEP reservoir isolated between 4478 ± 46 Ma and 4510 ± 10 Ma and pointing to long residence times in the lunar crust.

Despite the robustness of zircons, there is evidence of alteration during crustal modification processes. This is most obvious in the crystal structures. The fractured nature and abundance of shock metamorphic features in the lunar zircons demonstrate that these samples have experienced secondary impact shock modification over a range of shock pressures (e.g. Timms et al., 2012, 2017; Grange et al., 2013a, 2013b; Crow et al., 2019). Additionally, there is a small subset of zircons that exhibit late disturbance in the U-Pb system suggestive of multiple, <2000 Ma, Pb-loss events (e.g. Grange et al., 2013b; Crow et al., 2017). Most recently, U-Th-He ages were reported for a subset of Apollo 14 breccia zircons by Kelly et al. (2018). The zircons included in that study have ^{207}Pb-^{206}Pb ages between 3950 and 4332 Ma while the U-Th-He retention ages range from ~110 up to 3950 Ma and correlate with U and Th concentrations. The authors interpret the U-Th-He data as recording an impact event at 3950 Ma that caused total degassing of He and a subsequent overprint by a younger impact at 110 Ma, which induced He-loss in only the highest U concentration domains. The ability of zircons to record signatures of both primary crystallization and secondary modification makes lunar zircons interesting targets for investigating regolith modification processes.

1.2. U-Pu-Xe dating and xenon isotope systematics of zircon

U-Pu-Xe dating has not been applied to extraterrestrial zircons. This system of dating is based on the spontaneous fission of ^{238}U and ^{244}Pu to stable isotopes of xenon. Studies of terrestrial zircons have revealed that diffusion kinetics for xenon in non-metamict (i.e. crystalline) zircon are similar to those of lead (Shukolyukov et al., 1979, 1994; Pravdivtseva and , 1994; et al., 2009). However, in old samples with high U concentrations, and thus, high levels of crystal lattice damage, U-Xe ages are often younger than U-Pb ages (Turner et al., 2007). For instance, Turner et al. (2007) analyzed a suite of Hadean zircons from Jack Hills, Australia with ^{207}Pb-^{206}Pb ages between 976 and 4159 Ma, and obtained typically younger U-Xe ages ranging from 2510 ± 690 to 4950 ± 540 Ma. Most of these grains crystallized prior to the extinction of the short-lived radionuclide ^{244}Pu (half-life of 82 Ma; Ozima and Podosek, 2001), and as such their xenon isotopic compositions reflect mixing between both ^{238}U and ^{244}Pu fission components. The lunar zircons have ages indicative of crystallization while ^{244}Pu was still alive in the early solar system. Thus, an absence of xenon from ^{244}Pu fission within these ancient samples would indicate formation or complete degassing in the last ~4 billion years. Even in the case of complete degassing, a closure age is still accessible from the ratio between accumulated fission xenon from ^{238}U (half-life of 4472 Ma) and uranium content. In principle, this can be measured as the ratio between xenon produced by spontaneous fission of ^{238}U (S) and neutron induced fission of ^{235}U (N) if samples are irradiated in a reactor before analysis, similar to the ^{40}Ar-^{39}Ar dating method (Merrihue,

1965; Merrihue and Turner, 1966; Teitsma et al., 1975; Teitsma and Clarke, 1978). When just these two parents are considered, the age is noted as Xe_S-Xe_N. As with any chronometer, interpretation of the measured ages requires understanding of the response of the system to geological events; in the lunar context it is particularly important to determine how impact processes affect the Pu-U-Xe system.

Interpretation of U-Pu-Xe ages can be complicated by regolith processes. Fortunately, many of these processes produce distinct xenon isotopic signatures that potentially allow for their contributions to be identified and, in most cases, accounted for. For example, the ^{238}U to ^{235}U fission ratio can be affected by production of xenon from fission of ^{235}U induced by secondary neutrons in the lunar regolith. Regolith production of xenon by neutron induced fission of ^{235}U can in principle be detected by the presence of excess ^{129}Xe, which is also produced by neutron induced fission of ^{235}U via the intermediate radioactive precursor ^{129}I (half-life 16.1 Ma). In addition, zircons host rare earth elements which are targets for production of xenon by cosmic ray spallation – combining a measure of integrated exposure to cosmic rays with the production of xenon from ^{235}U potentially yields information about the timing of exposure and hence the history of the parent regolith sample (Turner et al., 2007).

Here we report xenon isotopic analyses of lunar zircons extracted from soil and breccia samples collected by the Apollo 14 mission. To realize the full potential of the system and optimize the extraction of information from the data, we developed a novel approach to data reduction applicable to multi-isotope systems comprising contributions from multiple processes. We demonstrate the potential of this technique to yield new insights into the evolution of the lunar crust and regolith. To validate our approach and to provide context we also report xenon isotopic analysis of zircons from the Vredefort impact structure, South Africa, where *inter alia*, we investigate the response of the U-Xe system in zircons to the high temperatures and high shock pressures characteristic of impact environments.

2. SAMPLES

2.1. Lunar

A set of large Apollo 14 zircons described in Taylor et al. (2009) and Crow et al. (2017) was chosen for xenon analyses. The grains were separated from two regolith soil samples (14163 and 14259) and two breccia samples (14305 and 14321). Because of the low average U concentration in Apollo 14 lunar zircons (~50 ppm), the zircons were chosen solely based on size and not parent sample characteristics. We also note that the zircons in this study are all >200 μm, and most are >300 μm, and all appear to be fragments from still larger parent grains (e.g. Crow et al., 2017). Fission recoil tracks in zircon are typically on the scale of 1–10 μm (e.g. Fish Canyon standard zircons; Brix et al., 2002), therefore we consider the recoil loss of fission derived xenon to be negligible for all the lunar grains studied. Because regolith zircons are typically larger than those recovered from breccia samples (e.g. soil grain 14259,664

Z1 is over 900 μm in diameter; Crow et al., 2017), the grains in this study were predominantly recovered from soil samples. A summary of the lunar samples is provided in the supplementary materials and relevant chronology is included in the discussion section. The reader is referred to Crow et al. (2017, 2019) for additional details on individual lunar zircons.

2.2. Vredefort

Five previously characterized samples from the Vredefort impact structure in South Africa were chosen to represent a range of pressure and temperature conditions associated with the impact cratering event. The target rocks at the Vredefort structure have formation ages ranging from ~2050 to 3300 Ma, whereas the impact crater has an established age of 2020 Ma (Spray, 1995; Kamo et al., 1996; Moser et al., 2011). The Vredefort zircons exhibit a range of responses to the cratering event and some zircons show additional disturbance due to a local intrusive event at ~1000 Ma (Reimold et al., 2000; Moser et al., 2011). In general, the Vredefort zircons have higher U concentrations than the lunar grains, ranging between 100 and 250 ppm (Moser et al., 2001, 2011; Moser, 1997). Below is a summary of the five Vredefort samples included in this study (Fig. 1 and supplementary materials).

Sample V49-2 is a foliated tonalite collected ~15 km from the geographic center of the impact and exhibits
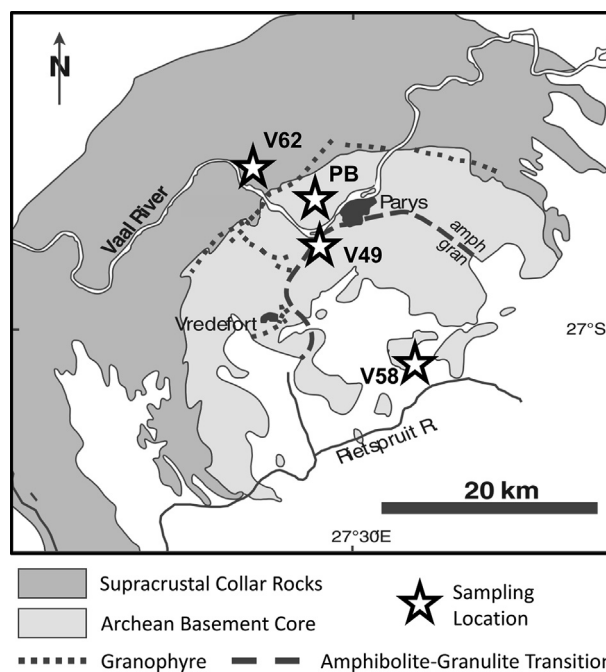

Fig. 1. Map showing sampling locations for Vredefort impact structure in South Africa. Samples represent a range of pressure and temperature environments including exposure high temperatures resulting recrystallization, high strain rates that produce shock microtwins, and post impact low-temperature thermal alteration. Figure is modified from Wielicki et al. (2012). See text and supplementary materials for description of individual samples.

amphibolite and granulite facies metamorphism (Moser et al., 2001). Zircons from V49-2 show up to ∼5% discordance in U-Pb ages and define a discord suggesting crystallization at ∼3100 Ma and minimal Pb-loss due to the Vredefort impact event (Moser et al., 2001).

Sample V58-1 is from a recrystallized norite dike near the geographic center of the impact structure (Moser, 1997). About 80% of the zircons from this sample are shocked and 20% are unshocked, prismatic grains. In this study, we analyzed euhedral grains from the unshocked zircon population. This population of grains has an average crystallization age of 2019 ± 2 Ma, consistent with the age of the impact event, and evidence for later Pb-loss associated with Kibaran mafic intrusions at ∼1000 Ma (Reimold et al., 2000; Moser et al., 2011).

Sample V58-2 is a leucogranofel from the same outcrop as V58-1 (Moser, 1997). Zircons from this sample all contain planar shock features and exhibit variable Pb-loss, however, there is no evidence of re-crystallized domains. The U-Pb data define a discord suggesting primary crystallization at 3293 ± 28 Ma and Pb-loss due to the Vredefort impact.

Sample V62 is an alkali feldspar granitoid collected ∼25 km from the impact structure center. This population of grains crystallized just prior to the impact event, 2077 ± 11 Ma, and contain microstructures that form at high strain rates characteristic of impact cratering (Moser et al., 2011; Morozova et al., 2017). Despite containing these features, the ages of V62 zircons appear to only be affected by the younger local intrusions and Pb-loss ages similar to V58-1.

We also included zircons from pseudotachylitic breccias (PB) collected 18 km from the impact structure center, which were previously analyzed by Wielicki et al. (2012). These grains yield crystallization ages between ∼2800 and 3000 Ma and show variable amounts of Pb-loss due to the impact event.

3. METHODS

The relationship between Xe_S-Xe_N dating and U-Xe dating parallels that between Ar-Ar and K-Ar. A fraction of ^{235}U is converted in a nuclear reactor to xenon by neutron induced fission, so the relative abundance of the parent and daughter nuclides can be determined by a single xenon isotopic analysis (provided that the $^{238}U/^{235}U$ ratio is known) (Shukolyukov et al., 1974). This section contains details on the neutron irradiation and laboratory analyses. In this work, contributions from possible fissile precursors (^{244}Pu, ^{238}U, ^{235}U) were derived from relative abundances of the heavy fissiogenic xenon isotopes (^{131}Xe, ^{132}Xe, ^{134}Xe and ^{136}Xe). Sufficient time was allowed after irradiation to allow complete production of these isotopes by decay of their radioactive precursors.

3.1. Irradiation and fluence monitoring

The lunar and terrestrial zircons were irradiated with thermal neutrons at the University of California Irvine (UCI) nuclear reactor during two separate sessions. The samples were accompanied by a fluence monitor, a glass that was created at University of California, Los Angeles (UCLA) specifically for this study. The samples were irradiated for 10 h with an average flux of ∼8×10^{12} n/cm^2/s, and allowed to cool for over six months prior to analysis. The UCI reactor flux is below the reactor flux used in the study by Turner et al. (2007), and therefore, production of excess ^{136}Xe by neutron capture on ^{135}Xe (a short-lived fission product of ^{235}U with half-life of 9.1 h) was not an issue. The composition and abundance of xenon in the standard glasses were measured in the Noble Gas Laboratory at ETH Zürich, and the reactor fluence was calculated by using the mass and U concentration of the glass (226 ppm). The calculated thermal neutron fluence for the two irradiations were 3.14×10^{16} and 5.1×10^{16} n/cm^2, respectively (see supplementary materials), which are within 15% of our expected fluences. The xenon isotope data for the irradiated UCLA standard glass are indistinguishable from reference values for ^{235}U fission yields from Ozima and Podosek (2001), but have higher precision (see Table 1). The values determined in this study therefore represent the best constraint, to date, on the xenon yields for fission of ^{235}U in geologic samples. More details on the standard glass and irradiation parameters can be found in the supplementary materials.

3.2. Xenon isotopic analyses

Xenon isotopic compositions of the zircons were measured using the Refrigerator Enhanced Laser Analyzer for Xenon (RELAX) at the University of Manchester, UK (Gilmour et al., 1992, 1994; Crowther et al., 2008). RELAX combines a resonance ionization ion source (Hurst et al., 1979; Payne et al., 1981) with a cryogenic sample concentrator and a time-of-flight mass analyzer. RELAX has a detection limit of ∼1000 atoms of xenon at the major isotopes, and is capable of achieving precision of ∼1% (1 σ) for major isotope ratios in samples with ∼10^5 atoms ^{132}Xe and the isotopic abundance of air Xe. The sensitivity of RELAX allows high precision spectral decomposition of xenon isotopic signatures when a single heating step releases ∼5×10^3 to 4×10^5 atoms.

Xenon analyses of lunar samples and of V58-2 were collected for individual zircons. Zircons from samples V58-1, V49-2, and V62, which have homogeneous levels of shock modification and U-Pb ages, were analyzed in groups of two to three grains in order to increase the xenon signal. Each sample was analyzed by incrementally increasing heating steps using a Nd:YAG laser (λ = 1064 nm) at currents between 13 A to 20.5 A (corresponding to a nominal range of ∼1 to 12 Watts). Zircons were heated directly (i.e. not in metal packets) and were melted or vaporized during the final heating step suggesting complete degassing of the grain. Sample analyses were bracketed by standard gas analyses (120,000 atoms ^{132}Xe of atmospheric isotopic composition) to track instrumental mass fractionation and sensitivity, and system blanks were collected at the beginning of each sample and after large gas releases. Unknown samples were not measured if the blank mass spectrum appeared to be more than roughly twice the average blank. Xenon isotope data are reported as numbers of atoms and

Table 1
Compositions of end member components used for deconvolution modeling.

End Member	^{124}Xe	^{126}Xe	^{128}Xe	^{129}Xe	^{130}Xe	^{131}Xe	^{132}Xe	^{134}Xe	^{136}Xe	Data Source
Solar Wind	0.00481 (6)	0.00417 (9)	0.0842 (2)	1.0401 (10)	0.1649 (4)	0.8263 (13)	1	0.3692 (7)	0.3003 (6)	Crowther and Gilmour (2013)
Air	0.00354 (1)	0.00330 (2)	0.07136 (9)	0.98320 (12)	0.15136 (12)	0.7890 (11)	1	0.3879 (6)	0.3294 (4)	Basford et al. (1973)
^{244}Pu	–	–	–	0.048 (55)	–	0.246 (20)	0.885 (30)	0.939 (8)	1	Ozima and Podosek (2001)
^{238}U	–	–	–	0.0006 (0)	–	0.0830 (6)	0.577 (1)	0.828 (1)	1	Ragettli et al. (1994)
^{235}U	–	–	–	–	–	0.454 (6)	0.672 (6)	1.230 (9)	1	This Work
^{235}U	–	–	–	0.1	–	0.453 (13)	0.677 (20)	1.246 (36)	1	Ozima and Podosek (2001)
REE Spallation	0.8935 (200)*	1	1.22(3)	1.6(4)	0.04(9)	1.64 (24)	0.06(7)	–	–	Hohenberg et al. (1981) & This work(*)
Ba Spallation	0.5447 (51)	1	1.621 (19)	1.6(4)	1.248 (31)	4.36 (11)	1.053 (22)	0.069 (14)	–	Hohenberg et al. (1981)

associated uncertainties at each isotope, where each corresponds to an original signal intensity, a correction based on a sensitivity factor determined from the air calibration, and a blank correction based on the equivalent signal in a procedural blank. For more information on the standard data reduction process used in this study, the reader is referred to the supplementary material.

4. DATA ANALYSIS AND RESULTS

A total of 295 xenon isotopic analyses of 15 lunar zircons and 29 Vredefort zircons were collected. A previous data reduction considered all releases and identified those from which ages could be obtained with sufficient precision to be meaningful (Crow, 2015; Crow et al., 2015). Because our approach to data reduction is computationally intensive, in this work we applied it to a dataset of 81 releases were chosen on the basis that the fractional error on the measured ^{132}Xe/^{136}Xe ratio was less than 3%; two extra analyses were added to this dataset for consistency with a previous report where a different approach was adopted (Crow, 2015; Crow et al., 2015 – detailed discussion of all releases may be found therein). A cut off value of 3% fractional error was chosen because at larger uncertainties the errors on sample ages are so large that geochronologically useful information cannot be obtained (e.g. samples with age uncertainties that span the age of the solar system). This dataset includes all analyses that previously yielded meaningful ages using a traditional approach. This dataset comprised 49 releases from 12 lunar grains and 32 releases from 15 terrestrial grains (or groupings of grains).

A complete record of data reduction including blank correction and calibration is available via the associated Mendeley dataset. The data are reported as atoms of each isotope in supplementary materials; these values have been corrected for instrumental blank contribution and mass-dependent fractionation. Almost all releases that comprise the final dataset in Table 2 had blank corrections that were less than 2% of the signal for the fission derived xenon iso-

topes (masses 131, 132, 134, and 136). The magnitude of blank corrections for the other isotopes varied depending on the amount of spallation, solar wind, or atmosphere in the release. For most samples, the lowest temperature steps were dominated by either air (Vredefort) or solar wind (lunar), while the high temperature steps were dominated by fission derived xenon with occasional contributions from spallation in the lunar samples. We developed a new approach to data reduction discussed below, but for illustrative purposes the measured xenon isotopic compositions are presented as three isotope plots normalized to ^{136}Xe in Figs. 2 and 3. Mixing lines between pure parent sources are included in the figures to illustrate the allowable isotopic compositions. For most of the samples, fission gas was released in one or two heating steps, and thus the concept of age plateaus does not have meaning for this dataset. Calculated ages are summarized in Table 2 and discussed in the text.

In Fig. 2 five releases from terrestrial zircons appear not to be consistent with mixing among expected components. In principle this may indicate the presence of an unanticipated component or an analytical artifact, we return to this below.

4.1. Component deconvolution in multi-isotope systems

In principle, it is expected that zircons from the lunar regolith that are subjected to artificial neutron irradiation may contain xenon from some or all of the following: spontaneous fission of ^{244}Pu, spontaneous fission of ^{238}U, neutron-induced fission of ^{235}U (reactor or regolith), cosmic ray spallation of rare earth elements, cosmic ray spallation of barium (with a variable contribution to ^{131}Xe after secondary neutron capture on ^{130}Ba), implantation from the solar wind, and/or contamination by the terrestrial atmosphere. Each of these source components has a distinct xenon isotope signature, as summarized in Table 1. Mono-isotopic excesses of ^{128}Xe from neutron capture on ^{127}I and ^{129}Xe (produced from fission via long-lived ^{129}I)

Table 2
Xe-Xe ages for lunar and Vredefort zircons.

Sample	Current (A)	SF/NF [**]	1σ	Xe_S-Xe_N Model Age (Ma)	1σ	[207]Pb-[206]Pb Age (Ma)	1σ	% Disc.
Irradiation 1								
14259_658 Z3	20.5 (F 5 min)[*]	7.2E−09	2.8E−09	990	390	4205	7	−3
	20.5 (F)	3.2E−08	6.7E−09	3500	740			
14259_658 Z6	16	3.1E−09	3.6E−09	440	510	4251	4	2
	20.5 (F)	2.0E−08	4.7E−09	2500	570			
	20.5 (F)	2.1E−08	2.2E−09	2500	270			
Irradiation 2								
14259_664 Z1	14	3.3E−09	4.5E−09	470	640	4075–4313	8	3/5
	14.5	1.5E−09	2.9E−09	220	430			
	15	1.4E−09	1.7E−09	200	250			
	15.5	5.3E−09	4.5E−09	740	630			
	16	2.1E−08	2.8E−09	2500	340			
	17	1.9E−09	5.2E−10	270	74			
	18	2.4E−09	8.8E−10	340	130			
	18 (F)	1.8E−08	1.1E−08	2200	1400			
	19	2.1E−09	1.4E−09	310	200			
	20.5	1.5E−09	3.2E−10	220	47			
14259_664 Z5	14	1.9E−09	2.7E−09	280	390	3932	9	0
	20.5	1.3E−10	2.7E−10	19	40			
14259_664 Z6	14	2.5E−08	3.7E−09	290	430	4338	3	0
	20.5 (F)	1.0E−09	3.1E−09	150	460			
14259_664 Z7	18	1.5E−08	6.9E−10	2000	88	4128	6	5
14259_664 Z11	12	9.6E−10	2.0E−09	140	290	4137	8	1
	14	2.6E−09	3.6E−10	380	51			
	20.5	2.7E−09	6.5E−10	400	93			
	20.5 (F)	4.6E−09	1.5E−09	650	210			
14259_664 Z12	12	1.2E−09	2.5E−09	170	370	4241	2	−1
	14	1.8E−09	2.4E−10	270	34			
	16	2.8E−09	3.8E−10	400	55			
	20.5	7.5E−10	5.8E−10	110	85			
	20.5 (F)	1.9E−10	6.9E−10	28	102			
14259_664 Z15	14	7.4E−10	1.2E−09	110	180	4327	4	3
	20.5	1.3E−10	2.4E−10	19	36			
14321 Z14	20.5	3.3E−08	1.3E−08	3600	1400	4134–4216	31/17	32/29
14321 Z20	2.5	4.4E−08	8.7E−09	4500	890	4241	5	5
V49-2 H1.1	14	2.5E−08	2.0E−09	2900	240	See Text		
	20.5	2.6E−08	1.9E−09	3000	210			
V49-2 H2.1	20.5	2.6E−08	1.8E−09	3100	200	See Text		
V49-2 H2.2	20.5	2.7E−08	2.8E−09	3100	320	See Text		
V49-2 H3.1	14	2.5E−08	3.3E−09	2900	390	See Text		
	20.5	2.7E−08	2.2E−09	3100	260			
	20.5 (F)	2.4E−08	3.7E−09	2800	430			
V58-1 H1.2	10%	1.1E−08	5.4E−09	1400	710	See Text		
V58-1 H2.1 + H3.1	20.5 (F)	1.6E−08	4.8E−09	2000	610	See Text		
	20.5 (F)	2.3E−08	7.1E−09	2700	840			
V58-2 Z2	20.5 (F)	1.9E−08	7.2E−09	2300	880	2001	12	1
V58-2 Z4	20.5 (F)	3.6E−08	1.7E−08	3900	1800	2573	10	15
V58-2 Z7 + Z8	20.5 (F)	2.2E−08	2.1E−09	2600	250	2842/2860	8/5	4/5
V58-2 Z9	20.5 (F)	2.5E−08	1.3E−09	2900	150	2689	8	5

Table 2 (*continued*)

Sample	Current (A)	SF/NF [**]	1σ	Xe$_S$-Xe$_N$ Model Age (Ma)	1σ	[207]Pb-[206]Pb Age (Ma)	1σ	% Disc.
V58-2 Z11	20.5 (F)	1.8E−08	5.7E−09	2200	710	2469	10	4
V62 H4.1	20.5	1.3E−08	6.7E−10	1700	87	See Text		
	20.5 (F)	1.7E−08	2.0E−09	2100	250			
V62 H5.1	20.5	1.5E−08	9.2E−10	1900	120	See Text		
V62 H5.2	14	1.5E−08	9.8E−10	1900	120	See Text		
V62 H5.2	20.5	1.6E−08	1.3E−09	2000	160			

[*] F = Focused laser beam. Heating time was 2 minutes unless otherwise specified.
[**] Ratio of spontaneous vs neutron induced fission. Determined using irradiation standard.

may also be present. For terrestrial zircons it is expected that only fission components and terrestrial atmosphere are present.

Typical approaches for the decomposition of components in noble gas isotopic data involve a series of corrections that, in effect, remove components from the measured signal until the desired quantities can be extracted. For instance, where samples are expected to be a mixture of solar wind and fission components, [130]Xe may be used to correct for the contribution of solar wind to the other isotopes because it is shielded from production by fission. In the general case, linear algebra can be used to determine the contributions from *n + 1* xenon components by using *n* isotope ratios and the requirement that the amount of a normalizing isotope be conserved. To continue the above example, after subtraction of trapped components (e.g. solar wind xenon or terrestrial atmospheric xenon), the relative contributions from three potential parent fissile isotopes ([235]U, [238]U and [244]Pu) can be calculated explicitly from any two of the [131]Xe/[136]Xe, [132]Xe/[136]Xe or [134]Xe/[136]Xe ratios (or two other independent ratios among these isotopes). However, error propagation requires careful attention when using this component subtraction and deconvolution method, partly because the uncertainties are correlated when ratios to a common denominator isotope are employed, and thus this complex data reduction protocol would introduce significant covariances among the derived quantities. More significantly, when the number of measured isotope ratios exceeds the number of mixing components (*n*), and choosing a subset of isotope ratios as the basis of a calculation fails to use all the available information.

To address these considerations, we adopted a forward modeling approach to component deconvolution of our measured mass spectra. We created model spectra consisting of linear combinations of some or all of the expected multi-isotope components, with each component's contribution parameterized by the number of atoms (N) each made at its normalizing isotope ([132]Xe for solar wind and air xenon, [136]Xe for fission components, [126]Xe for spallation components). This is necessary because there is no one isotope of xenon that is common to all components (see Table 1). The models also allowed for potential linear mass fractionation of the mixture resulting from measurement conditions and/or contributions to be forced to be

positive. The amounts contributed by each component were varied until chi-squared, $\chi^2 = \sum_i \left(\frac{N_{i,measured} - N_{i,modeled}}{\sigma_i} \right)^2$ where i is a given isotope of xenon, was minimized between the modeled and measured spectra. (Minimization was done using the Solver™ add in for Microsoft Excel™). It was possible to include all, or a subset, of the available isotopes. This allowed for the presence of monoisotopic contributions (e.g. [131]Xe production produced after neutron capture on [130]Ba) to be assessed by excluding the daughter isotope from the calculation of chi-squared and determining the difference between the measured and modeled atoms of the excluded isotope. A monoisotopic contribution would present itself as an excess in the measured above the modeled atoms.

Variances of, and covariances among, the source contributions and calculated excesses were assessed by conducting 100 model fits for each measurement, in which synthetic spectra were generated for the measured and components using a Monte Carlo approach. We assumed the measured (or reported) values and analytical errors correspond to the center and full-width at half maximum of an independent normal distribution, respectively. This procedure was conducted for every isotopic analysis in the dataset of large releases. Model fits were deemed acceptable where the minimum chi-squared per degree of freedom of the model against the data (MSWD hereafter) was less than two; the variances and covariances of mixing parameters for acceptable model fits with MSWD greater than 1 were scaled by the MSWD of the best fit model. Isotope ratios and their associated measurement error are based on the mean and standard deviation of a distribution. Neither is exact, they are estimated from a series of repeat measurements. One hundred iterations of a Monte Carlo are sufficient to ensure that the uncertainty is dominated by the uncertainty in the quantities estimated from the data (the average and the standard deviation).

In this approach, an acceptable fit between the model and data is achieved when the data are consistent with mixing among the expected components and there is no evidence for an additional component or artifact affecting the data. In such cases we use the parameters of the best fit model as estimates of the numbers of atoms from each component contributing to the release. This is the same logic as employed in isochron dating in which a model that

includes a single closure age predicts a correlation between parent element and daughter isotope; an attempt is made to fit such a model to the data, and if the best fit model has an acceptable MSWD, the gradient of the line is interpreted chronologically.

To pursue the analogy, where an isochron is not observed, or when a trend appears to be present but MSWD is unacceptable, further examination may be made to determine the underlying cause and, in some cases, outliers are rejected. Similarly, in our approach, we considered

what factors outside the model might have affected the observed composition. Such factors potentially include a contribution of xenon from an unanticipated or unknown source or an experimental issue. Our approach was to consider unexpected xenon contributions only if an experimental issue could be ruled out. However, it should be emphasized that a large majority of the releases yielded acceptable model fits in both the terrestrial and lunar datasets.

4.2. Data reduction

4.2.1. Vredefort zircons

Our study of these terrestrial samples allows us to investigate the effects of a major impact event on the U-Xe system. However, the analyses also served to test the experimental approach since the history of the samples is well constrained; their crystallization ages preclude the presence of xenon from fission of ^{244}Pu, and their residence at or below the Earth's surface precludes the presence of xenon from spallation of rare earth elements (expected trace elements in zircons) or barium (not expected as a trace element in zircon, but potentially present in inclusions). An ideal data reduction process would identify cases where the model failed to include a process or component affecting the data, allow quantification of contributions from expected components, and return contributions within error of zero for components that could not possibly be pre-
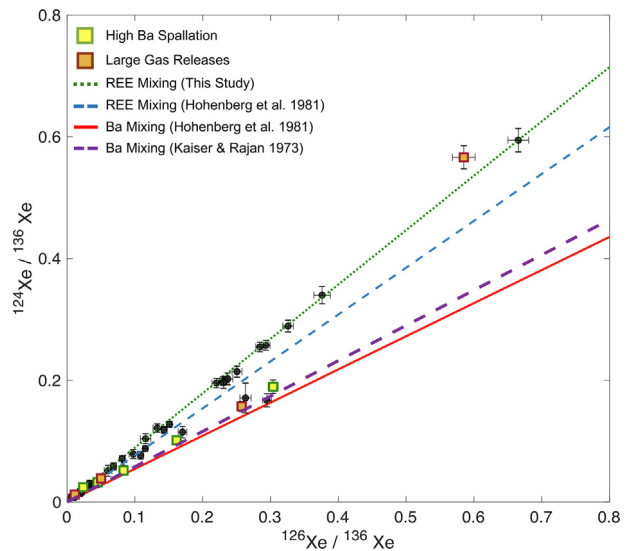

Fig. 2. Xenon isotopic data for Apollo 14 and Vredefort zircons, for which appreciable fission gases were identified, illustrating mixing between parent components. Almost all grains contain contributions from solar wind or air. Data that fall outside of the allowable compositions are attributed to large gas releases or hydrocarbon interferences. The results of the component deconvolution modeling suggest that there is no contribution from ^{244}Pu in either the lunar or terrestrial zircons. The relative contributions from ^{238}U and ^{235}U fission were therefore used to determine Xe$_S$-Xe$_N$ ages, which are presented in Fig. 4.

Fig. 3. Apollo 14 zircon data shown as spallation dominated isotopes ^{124}Xe and ^{126}Xe relative to fission dominated ^{136}Xe for each temperature extraction. The Ba spallation compositions (red solid line and purple dashed lines) are consistent with the Ba dominated analyses. However, the rest of the data are not consistent with the REE spallation composition from Hohenberg et al. (1981). This could be due to differences in relative REE compositions or cosmic ray energy spectrum between the lunar zircons and Angra dos Reis meteorite. A new spallation composition, appropriate for the lunar zircons, was defined in Section 4.2.2 for the component decomposition modeling (green dashed line).

sent. In effect, the Vredefort samples serve as a secondary standard testing our analytical and data reduction procedures. The approach to data reduction is summarized here and discussed more extensively in Supplementary Material section S6.

In general, the goal of the component deconvolution was to determine the best model fit to the data using the least number of components allowed by the data. This was done by first determining a model fit using the maximum number of logical components. If any of the components had a contribution within error of zero, a model fit was redone excluding this component(s) as a possible source of xenon. As a test of our approach, we first considered the unphysical, possibility that spallation xenon contributed to the gas released from Vredefort samples. In acceptable model fits including xenon from air, fission and spallation (total of six components, with no mass fractionation) excluding mass 128 (where a hydrocarbon interference is sometimes present in RELAX, as discussed below), the calculated contributions of spallation ^{126}Xe from Ba and REE targets were always within error of zero, as expected.

As a further test, model fits were then repeated excluding all the isotopes that may be present as monoisotopic excesses and allowing only xenon from fission and air to contribute (four components). There were no significant excesses at masses 129 or 131 in acceptable model fits, indicating no contributions from ^{129}I and ^{130}Ba, and the contribution from ^{244}Pu fission was always within error of zero. Once again, the data reduction process yields the expected result.

Model fits were repeated excluding both the spallation and ^{244}Pu fission components, and using all isotopes (apart from ^{128}Xe) to calculate MSWD. Of the 32 releases selected for reduction, 8 failed to meet our criterion for a good fit (MSWD < 2). Of these, two had nominal ^{132}Xe amounts in excess of 2.5×10^6 atoms of ^{132}Xe (>20x larger than the RELAX calibration aliquot – other releases were $<7.5 \times 10^5$ atoms of ^{132}Xe) and exhibited signs of peak broadening when the source spectra were analyzed.

All but one of the remainder had nominal excesses at mass 128 that would correspond to more than 3000 xenon atoms, whereas none of the releases with acceptable model fits indicated the presence of such an excess. RELAX uses a high intensity ultraviolet laser pulse to resonantly ionize xenon, this pulse is also capable of non-resonant ionization of hydrocarbons. The largest mass peak in the xenon region from this process is observed at mass 128. Ambient levels of hydrocarbons in the mass spectrometer contribute to the procedural blank and their effect is accounted for in the blank correction. However, samples can introduce additional hydrocarbons. In particular, when samples have been mounted for probe analysis, as here, occasional incomplete removal of the resin after demounting can lead to a larger input of hydrocarbons on laser heating. Uniformly adopting much longer gettering times might mitigate this effect in samples affected, at the expense of a larger blank for all releases that would preclude interpretation of the data.

Generally, releases failed to yield an acceptable model fit if and only if the ^{132}Xe release was greater than 2.5×10^6

atoms or there was evidence of hydrocarbon contamination. There were two exceptions. One release (V49-2 H2.1 20.5A 2mins) gave χ^2 per degree of freedom of 2.2 with a ^{132}Xe release of 3.3×10^5 atoms and no evidence of hydrocarbons; this is considered to be a statistical fluctuation. Another (V62 H4, 20.5AF 2mins) yielded an acceptable fit only when a degree of linear mass-dependent fractionation was allowed (15.3 ± 3.5 ‰ u^{-1} favoring the light isotopes). We note that the input data for the model fits was already corrected for expected instrumental mass fractionation using the air calibration analyses; this sample required fractionation above that expected from the air calibration. Having observed this potential effect in one sample, the other releases were reanalyzed allowing mass fractionation. In no other case did the optimum model fit require additional mass fractionation, but this reduction represents our finalized dataset. Allowing the possibility of mass fractionation slightly increases the errors on reported quantities.

Our study of the Vredefort dataset demonstrates that adopting a criterion based on MSWD reliably excludes analyses affected by hydrocarbon contamination (i.e. those with excesses at mass 128), and such a criterion was adopted for the study of lunar zircons. Releases from the Vredefort dataset that yielded acceptable model fits were used to derive U-Xe model ages based on the best fit abundances of ^{136}Xe from ^{238}U and ^{235}U, their variances, and the covariance between them.

4.2.2. Apollo 14 zircons

Fig. 3 indicates the presence of two distinct, well-separated components contributing to low-mass xenon isotopes in releases from the lunar zircons. Our working assumption was that these corresponded to the two principal spallation targets. One has relative contributions to ^{124}Xe and ^{126}Xe consistent with barium spallation. Barium is not an expected trace element in zircon but may be present in inclusions or accessory phases. The lunar zircons have been shown to host impact melt inclusions, which are a potential source of barium spallation xenon (Crow et al., 2019). A spallation component from rare earth elements is expected in zircons based on trace element chemistry. However, the second spallation component has a higher ^{124}Xe/^{126}Xe ratio (0.89 ± 0.02) than that inferred for rare earth element spallation in Angra dos Reis (0.770 ± 0.015) by Hohenberg et al. (1981) (Fig. 3). We hypothesized that this ratio is representative of REE spallation in zircon under the conditions in the lunar regolith and adopted the ratio implied by our data for this component.

Given this observation, other isotope ratios may deviate from the accepted composition of REE spallation, notably ^{128}Xe, ^{129}Xe and ^{131}Xe (production of ^{130}Xe by spallation of rare earth elements is low) (Kaiser and Rajan (1973); Lugmair and Marti 1972). To account for this possibility and because monoisotopic contributions are potentially present at these masses, four sets of model fits were attempted for each release: first, ^{128}Xe, ^{129}Xe and ^{131}Xe were all excluded; second, only one of the three isotopes was included; third, each combination of two monoisotopic components was attempted; and finally, all nine isotopes

were included. It became apparent that one zircon (Z12 from 14259,664) showed evidence of excess ^{129}Xe produced after fission of ^{235}U induced by secondary neutrons in the lunar crust. Since this is potentially an important tracer of lunar regolith history finalized data reductions excluded this isotope so excesses of ^{129}Xe could be identified.

Eight releases from five zircons required a significant contribution from spallation of rare earth elements. In these cases, fits to $^{124, 126, 130, 132, 134, 136}$Xe predicted more ^{128}Xe, ^{129}Xe and ^{131}Xe than was observed. The observed deficits correlated with the amount of ^{126}Xe from this spallation source (Supplementary Material Fig S4 and Table A4), indicating that the REE spallation composition used in this model (i.e. Angra Dos Reis) has higher $^{128, 129, 131}$Xe/^{126}Xe ratios than that present in the samples. The spallation composition for REEs implied by the observed correlations is listed in Table 1. The composition is close to that reported by Hohenberg and Rowe (1970) for a rare earth mixture approximating the composition of Angra Dos Reis artificially irradiated with 730 MeV protons (Supplementary Fig. S5), suggesting production is primarily by low energy protons and so indicating a period of deep burial in the regolith that dominates the spallation signature. Four other releases showed a significant contribution from spallation of Ba – three of these releases also exhibited the largest excesses of ^{131}Xe, which is produced from ^{130}Ba after neutron capture (Supplementary Material Fig S6). There was some indication of a variation from the Angra dos Reis barium spallation signature (Hohenberg et al., 1981), but these were at a low level of significance and not considered further (Supplementary Material).

For each release, the data reductions used to test for the presence of ^{244}Pu or to examine U-Pu-Xe ages consisted of the acceptable model fit that included the most isotopes apart for ^{129}Xe. Evidence for the presence of xenon from ^{244}Pu would consist of releases where the inclusion of this component was necessary to produce an acceptable fit. Twenty releases (out of 49) yielded acceptable model fits to all the isotopes. Fifteen required both ^{128}Xe and ^{131}Xe to be excluded, of which 12 were releases that showed a significant contribution from spallation at ^{126}Xe. Five required only ^{131}Xe to be excluded. Two required only ^{128}Xe to be excluded. Seven releases did not produce an acceptable model fit. Fits to these releases were repeated including ^{244}Pu as a component and allowing for the possibility of mass fractionation. Two resulting acceptable model fits required a contribution from ^{244}Pu at the 2σ level, which is consistent with random variation around the mean in 49 samples. Fits were also attempted with the assumption that xenon from the terrestrial air, rather than solar wind, contributed to the trapped component. This resulted in slightly lower overall contribution from fission components, but still no evidence for a contribution from ^{244}Pu. Thus, there is no compelling evidence for a contribution from ^{244}Pu in any of the lunar zircons.

4.3. Xe$_S$-Xe$_N$ ages

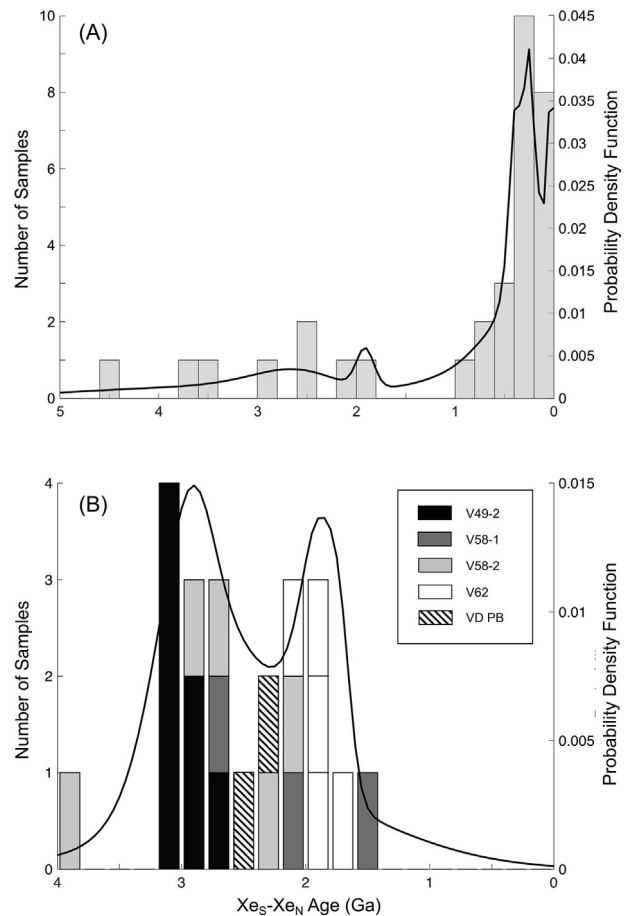In this section, we discuss model Xe$_S$-Xe$_N$ model ages for all releases that resulted in acceptable model fits. Details

Fig. 4. Xe$_S$-Xe$_N$ age histograms and probability functions for Apollo 14 (A) and Vredefort (B) zircons. The Vredefort ages (B) are broadly consistent with the zircon U-Pb ages, suggesting xenon and lead diffusion kinetics are similar in the conditions experienced by impact crater basements. In contrast, the Apollo 14 zircons (A) are characterized by an abundance of ages <1000 Ma, suggesting other regolith gardening processes are influencing the Xe$_S$-Xe$_N$ distribution. Probability density functions are subsampled at 10 Mas.

on calculating Xe$_S$-Xe$_N$ ages and unceratinties can be found in the Supplementary Materials. Neither the lunar nor the terrestrial datasets requires a contribution from ^{244}Pu, so Xe$_S$-Xe$_N$ ages were calculated from the ratio of contributions to ^{136}Xe from ^{238}U spontaneous fission and neutron induced fission of ^{235}U, assuming that the latter was entirely produced in the reactor irradiation. Errors on the ages include a contribution from the covariance between the two quantities. Histograms and probability density functions for the Xe$_S$-Xe$_N$ ages are presented in Fig. 4 and summarized in Table 2.

4.3.1. Vredefort

Although our dataset was selected based on sufficient gas to measure the ^{136}Xe/^{132}Xe ratio to better than 3%, some Vredefort releases were dominated by xenon from the Earth's atmosphere and the amount of ^{136}Xe from ^{235}U was within 2σ of zero. These releases are not discussed

further. The remaining dataset, consisting of 17 analyses of ten zircons, tests the reproducibility of the technique. This is demonstrated by the reproducable ratio of atoms ^{136}Xe from ^{238}U spontaneous fission vs. ^{136}Xe from ^{235}U induced fission for samples of similar geologic histories (Fig. S3 in the supplemental materials). Six releases from four zircons from site V49 (Pb-Pb crystallization age ~3100 Ma – Moser et al. (2001)) yield consistent ages indicating closure at 2995 ± 100 Ma (weighted average, 1 σ error), consistent with little or no xenon loss post-formation. Five releases from 3 zircons from site V62 yield precise ages, which are self-consistent and indicate closure at 1840 ± 55 Ma (Pb-Pb crystallization age 2077 ± 11 Ma; Moser et al., 2011) suggesting this sample has experienced partial Xe-loss due to the more recent ~1 Ma event, which also affected their U-Pb system. Zircons from both V58-2 and PB samples have weighted mean Xe_S-Xe_N ages between the U-Pb crystallization ages and the Vredefort impact event; 2773 ± 126 and 2432 ± 219, respectively. Two samples from V58-1 yielded a weighted mean age of 1979 ± 404, which is consistent with the age of the Vredefort impact event at 2020 Ma (Spray, 1995; Kamo et al., 1996; Moser et al., 2011). The general agreement between the U-Pb and Xe_S-Xe_N systematics suggests that xenon and lead exhibit similar diffusivity under the conditions experienced by the Vredefort zircons and validates our approach to data reduction.

4.3.2. Lunar

Unlike the terrestrial samples, the lunar zircons have Xe_S-Xe_N model ages significantly younger than the ^{207}Pb-^{206}Pb ages, the latter of which are all older than ~3900 Ma. The majority of the lunar grains have Xe_S-Xe_N ages less than 1000 Ma, with a small clustering around ~2000 Ma. There are a few samples with ages older than 3000 Ma, however the uncertainties are large (>1000 Ma). Only two of the grains analyzed were from breccia samples, and both yield Xe_S-Xe_N ages older than 3600 Ma for the highest temperature steps. This may suggest a systematic difference in ages between the soil and breccia grains, but confirmatory data are needed.

5. DISCUSSION

The contrasting distribution of Xe_S-Xe_N ages for the Vredefort and Apollo 14 samples suggest drastically different processes affecting zircons in the terrestrial and lunar environments. Unlike the Earth, the Moon's surface is continually processed by high energy particle bombardment, significant diurnal heating, and impact gardening. Below, we explore what the zircon xenon record reveals about the effect of these processes on lunar surface materials.

5.1. Thermal stability of Xe_S-Xe_N dating in zircon

The U-Xe (or Xe_S-Xe_N) dating technique was detailed by Shukolyuko et al. (1974), Teitsma et al. (1975), Teitsma and Clarke (1978), et al. (1979), Meshik et al. (1987), Reimold et al. (1995) for application to zircon and other uranium bearing minerals. Since then, only a handful of studies have utilized Xe_S-Xe_N dating of individual

zircons or studied the diffusion kinetics of xenon in zircon (. For many of these studies, there has been surprising concordance between the U-Pb and U-Xe systems suggesting a similar retentivity of lead and xenon in zircon over geologically relevant conditions (e.g. Shukolyukov et al., 2009). This conclusion is reinforced by the Xe_S-Xe_N ages of the Vredefort impact zircons reported herein. The U-Pb analyses of V49 and V58-2 zircons indicate crystallization between 3292 ± 28 and 3092 ± 7 Ma and partial Pb-loss due to the high temperatures during and just following the Vredefort impact event at 2020 Ma. For the zircons that produced sufficient fission xenon, these samples record Xe_S-Xe_N ages of 2995 ± 100 Ma and 2773 ± 126 respectively. Small amounts of recrystallization have been observed in grains from both samples (Moser, 1997; Moser et al., 2001), which requires temperatures of ~900–1000 °C or above (Weber, 1990; Weber et al., 1994; Reimold and Gibson, 1996). This suggests that in case of recrystallization, both lead and xenon may be lost from zircon. Sample V62 crystallized at 2077 ± 11 Ma and subsequently experienced the impact event at 2020 Ma. While the sensitivity of the xenon system is too coarse to be able to detect Xe-loss so soon after formation, V62 was chosen to investigate the effects of subsequent hydrothermal alteration resulting from magnotectonic activity at ~1000 Ma (e.g. Reimold et al., 1995, 2000). A lower Concordia intercept of 1016 ± 110 Ma and Xe_S-Xe_N ages of 1840 ± 55 Ma suggest that both the U-Pb and U-Xe systems experienced daughter isotope loss during this event. The maximum temperatures associated with this local intrusive event are estimated to be between ~150 and 300 °C (Baughman and Flowers, 2018). The results of Vredefort impact zircons provide further evidence of the high thermal stability of the U-Xe system, and suggest that the diffusivity of xenon and lead are similar in zircon under typical crustal conditions.

5.2. Effects of lunar surface irradiation

Samples on the surface of the Moon are potentially subject to a range of additional alteration due to high energy particle bombardment which is known to affect xenon isotopic compositions of lunar soils and meteorites (e.g. Marti et al., 1970; Podosek and Huneke, 1971; Podosek et al., 1971). All lunar zircons in this study produced at least one release with an appreciable spallation xenon component produced by exposure to cosmic rays during residence near the Moon's surface. The flux of high energy particles is thought to peak at a depths between ~50 and 100 g/cm^2 for <100 MeV and at progressively shallower depths for higher energies, with the flux for >1 GeV particles peaking at the lunar surface (Lingenfelter et al., 1972; Reedy & Arnold, 1972). The flux of thermal neutrons peaks slightly deeper at ~150 g/cm^2, however, the peak is relatively broad and there is appreciable thermal neutron flux at shallower depths where higher energy particles peak (i.e. between 50 and 100 g/cm^2). This suggests that the lunar zircons that show evidence of cosmic ray spallation were likely also exposed to thermal neutron irradiation. Since the Xe_S-Xe_N dating method relies on thermal neutron irradiation within a nuclear reactor to infer U concentration, an addi-

tional neutron fluence on the lunar surface could result in an overestimation of ^{235}U concentration and an underestimation of Xe_S-Xe_N age. The error due to neutron exposure on the lunar surface neutron fluence would only be significant if the total thermal neutron fluence is comparable to the reactor irradiation dose, or if the surface irradiation was ancient when concentrations of ^{235}U were significantly higher.

There are three ways to assess if surface neutron exposure is significantly biasing the young Xe_S-Xe_N ages to younger values. First, we measured the xenon isotopic composition of two unirradiated zircons from breccias 14,305 and 14,321, and the fission gases are consistent with a mixture between solar wind, REE spallation, and ^{238}U fission (data are reported in supplementary Table S5). The observation of a spallation component and a lack of a ^{235}U fission signature (i.e. the lack of an excess in ^{129}Xe in all but one zircon) suggest that the surface thermal neutron irradiation is not significant for breccia samples. We also attempted to measure xenon from a third unirradiated grain from soil 14163, however, the gas yields were too low to be accurately measured. Second, we looked for a correlation between spallation xenon content with either ^{235}U derived xenon or Xe_S-Xe_N age, but we found none. This means the apparently young samples do not have a significantly higher spallation component than the more ancient samples. However, the REE concentrations in lunar zircons vary by over an order of magnitude (Nemchin et al., 2010; Hopkins and Mojzsis, 2015, Crow et al., 2017), so the magnitude of spallation xenon may instead represent variations in REE concentration and not the extent of surface exposure.

Third, the absence of an excess of ^{129}Xe in all but one lunar zircon can be used to place limits on the exposure to thermal neutrons on the lunar surface (Meshik et al., 1987; Geyh and Schleicher, 2012). The relative yield of products with mass 129 to mass 136 from thermal neutron induced fission of ^{235}U is ~ 0.0861. The instantaneous products are predominantly radioactive, and decay through a sequence of intermediate daughters that ultimately result in stable ^{129}Xe and ^{136}Xe. While the half-life of the mass 136 decay chain is on the order of minutes, the mass 129 decay chain is significantly longer due to the 16.1 Ma half-life of ^{129}I (Ozima and Podosek, 2001). Using the Bateman equations for decay series (Bateman 1910), we can calculate the $^{129}Xe/^{136}Xe$ as a function of surface exposure. For example, the $^{129}Xe/^{136}Xe$ ratio reaches about 0.0775 (90% the final cumulative yield) after 228 Ma regardless of the thermal neutron flux. Thus, the lack of measurable ^{129}Xe excess requires that any lunar surface exposure to be relatively recent (<200 Ma) or to be small such that the contribution to ^{136}Xe is negligible. To demonstrate this point, and to place an upper limit on the contribution of neutron exposure on the lunar surface to production of ^{136}Xe from ^{235}U fission, we determined the maximum allowable thermal neutron fluence, assuming the upper limit on excess ^{129}Xe can be approximated by the uncertainties on the measured ^{129}Xe atoms for each sample. This was done for all samples that did not show an excess in ^{129}Xe, and assumed assume a thermal neutron flux of $\sim 2n/cm^2/$

sec which is near the upper bound estimated by Lingenfelter et al. (1972) and Woolum and Burnett (1974). The maximum allowable exposure ages for these samples range from 94 to 774 Ma, and associated correction to Xe_S-Xe_N ages results in a maximum shift of +138 Ma. Although the modeled surface exposure age greatly relies on the assumed thermal neutron flux, the corrected Xe_S-Xe_N ages are less affected by changes in thermal neutron flux. This is because the correction is limited by the total fluence (i.e. total number of thermal neutrons) and the independent fission yields. This suggests that surface exposure to thermal neutrons cannot account for the abundance of young Xe_S-Xe_N ages in the lunar zircons (see supplementary materials for more details). However, to fully take advantage of this modeling, precise ^{129}Xe yields of REE spallation must be determined.

The one sample for which an excess ^{129}Xe was measured (14259,664 Z12) requires a different exposure history than the rest of the Apollo 14 zircons in this study. We conducted the same modeling as discussed previously, and found that 14259,664 Z12 needs at least factor of three higher thermal neutron flux on the lunar surface to account for the $^{129}Xe/^{136}Xe$ ratio. This can be accomplished by an actual variation in flux, or, more realistically, surface exposure much earlier in lunar history when the relative concentration of ^{235}U to ^{238}U was higher. This would be consistent with the observation that this sample has an unusually high contribution of ^{136}Xe from ^{235}U relative to ^{126}Xe from REE spallation (see supplementary materials for more details). We, therefore, interpret this grain to have ancient surface exposure, after which it was subsequently buried, and then finally excavated by a young impact event and deposited at the Apollo 14 landing site. Like the other lunar zircons in this study, the contribution ^{235}U from of the recent surface exposure would be minimal compared with the ancient exposure and the rector induced fission.

5.3. Regolith gardening processes

Two other processes may influence the differences between breccia and regolith zircon ages: diurnal heating and impact gardening. The effect of lunar diurnal heating is of concern for other noble gas based geochronologic systems, for example, evidence of diurnal Ar-loss has been observed in multiple Apollo samples (e.g. Turner, 2008; Gombosi et al., 2015; Shuster and Cassata, 2015). Diurnal heating was also considered by Kelly et al. (2018) as a way to explain the range of U-Th-He ages obtained for lunar zircons in Apollo breccia 14311. The authors conducted forward modeling of diurnal heating effects and concluded that residence on the lunar surface upwards of 660 Ma was necessary to explain the U-Th-He age distribution. Additionally, zircons within breccias >0.5 m in diameter, or buried in the regolith below ~ 10 cm, would experience marked dampening of diurnal heating (Hayne et al., 2017). For these reasons, Kelly et al. (2018) ruled out diurnal heating as a significant influence on the U-Th-He data. Most of the zircons reported herein were extracted from soils collected within the top 10 cm of the surface, therefore, the recent diurnal heating of soil zircons would

be greater than the heating of the breccia zircons. However, we expect the diffusion kinetics of xenon to have much higher activation energies than Ar and He, similar to those of lead in non-metamict grains, at maximum diurnal temperatures. Additionally, all of the lunar zircons retain ancient (>3.9 Ga) U-Pb and ^{207}Pb-^{206}Pb ages with little to no evidence of more recent Pb-loss (e.g. Crow et al., 2017) making the young U-Xe ages of the soil zircons are difficult to explain by diurnal heating alone. However, further investigation of the U-Xe ages of lunar breccia zircons and U-Th-He ages of soil zircons would be useful in fully understanding the effects of diurnal heating on these geochronologic systems.

Micrometeorite impacts and regolith gardening processes would likely have a stronger influence on the soil grains relative to those hosted in breccias, since the breccia zircons are more thermally and mechanically shielded by the host rock. Shock induced resetting or disturbance has been shown to affect whole rock ^{40}Ar-^{39}Ar, Rb-Sr, and U-Pb ages (Cassata et al., 2010; Gaffney et al., 2011; Boehnke et al., 2016). Of particular interest is the observed high-temperature Ar-loss in many meteorite and Apollo samples, which has been attributed to impact shock heating of multiple phases with different Arrhenius relationships (e.g. Cassata et al., 2010; Boehnke et al., 2016). It is possible that a similar relationship may exist where diffusion of xenon and lead in zircon are comparable at typical upper crustal conditions, however, the difference in diffusion rates becomes more pronounced at extremely high temperatures. Further investigation of the diffusion kinetics of Xe-in-zircon and shock experiments are necessary to completely understand the effects of regolith gardening the U-Xe system in zircon.

5.4. Interpretation of zircon lunar Xe$_S$-Xe$_N$ ages

In this section, we consider only releases where the uncertainties on the Xe retention ages are less than ~1000 Ma (in effect, where there was sufficient fission xenon and a relatively small contribution from solar xenon). Let us first discuss the maximum Xe$_S$-Xe$_N$ model ages for each zircon. Two zircons give distinctly old Xe$_S$-Xe$_N$ ages; soil grain 14259,658 Z3 and breccia grain 14321 Z20 yield ages of 3512 ± 742 and 4483 ± 888 Ma, respectively. These ages are within uncertainty of the ^{207}Pb-^{206}Pb crystallization ages, however, the absence of ^{244}Pu derived xenon requires that the samples were completely degassed after ~3900 Ma or the Pu/U ratios of the zircon forming magmas were significantly lower than on Earth. Our data from these samples are consistent with xenon retention since crystallization. There is a second set of four zircons that give degassing maximum model ages between 1900 – 2800 Ma (14259, 658 Z6, 14259,664 Z1, Z6 and Z7). There is no significant magmatic event known to occur on the Moon during this time period, which suggests these samples record one or more impact events during this time. Similarly aged event at 1940 ± 10 Ma and 1733 ± 130 Ma (2 σ) were also observed in zircons from Apollo 15405, which resulted in up to 40% discordance in U-Pb ages for some samples (Grange et al., 2013b).

All of the other releases yield Xe$_S$-Xe$_N$ model ages younger than 1000 Ma implying that these samples all experienced significant, recent Xe-loss. There are young impacts on the Moon, such as Tycho and Copernicus, that have been implicated in resetting U-Th-He ages and inducing recent Pb-loss (<1000 Ma) in the lunar zircons (Crow et al., 2017; Kelly et al., 2018). In light of the discussion above, we currently favor the constant bombardment of the regolith by small impactors that are as an explanation for the Xe$_S$-Xe$_N$ ages of the regolith zircons. Whether these model ages reflect complete degassing in a recent impact at a well-defined time or cumulative loss due to micrometeorites and regolith gardening processes, is difficult to distinguish with the current dataset. In the case of either partial or total degassing, the Xe$_S$-Xe$_N$ ages represent upper limits on the surface exposure or degassing ages. This implies that the lunar regolith zircons contain a record of the recent impact history of the lunar surface.

The preponderance of <1000 Ma ages may not indicate a recent uptick in the number of impact events or regolith gardening, but could instead reflect a sampling bias resulting from the way in which regolith samples were collected by Apollo astronauts. A similar age bias has been invoked by Huang et al. (2018) to explain the ^{40}Ar-^{39}Ar age distribution of impact glass spherules (Zellner et al., 2009). This study found that the age distributions of impact glass in soil samples should vary with depth based on impact ejecta modeling. Additionally, the authors concluded that collection of material from only the top 10 cm of regolith would introduce a bias towards young, <1000 Ma ages. Since most of the lunar zircons in this study are derived from similar depths, this bias could also be manifest in the Xe$_S$-Xe$_N$ age distribution. As such, the histograms in Fig. 4A could represent the lifetime against resetting for a zircon in the lunar regolith.

6. SUMMARY AND CONCLUSIONS

We presented the first xenon isotopic analyses and Xe$_S$-Xe$_N$ ages for zircons from lunar samples. We also conducted similar analyses on a suite of zircons from the terrestrial Vredefort impact structure to investigate the effects of basin forming impact events on xenon systematics in zircon. The terrestrial samples yield an expected combination of fission-derived and atmospheric components, and the Xe$_S$-Xe$_N$ ages are largely consistent with those of the U-Pb system. This suggests the diffusion kinetics of Xe-in-zircon are similar to that of Pb under the temperature and shock-pressure regimes experienced by sub-crater floor samples. A very different behavior is observed in the lunar samples in which the Xe$_S$-Xe$_N$ ages are consistently younger than the U-Pb and ^{207}Pb-^{206}Pb ages. We believe that the inconsistency between the lunar and terrestrial samples is mostly likely due to differing impact regimes between the sub-crater floor and the lunar regolith, which is predominantly composed of impact ejecta. In addition, the lunar regolith samples are exposed to repeated micrometeorite bombardment, which could have a cumulative degassing effect that would eventually result in young ages commensurate with ages determined from cosmogenic nuclides. The two breccia

zircons in this study yielded Xe_S-Xe_N ages within error of their [207]Pb-[206]Pb ages, which are also significantly older than the soil zircon ages. This may suggest that the host breccia adequately dampens regolith processes so that ancient Xe_S-Xe_N ages can be preserved. However, given the number of breccia zircons were successfully dated in this study, further investigation of these samples is necessary. The lack of plutogenic xenon (i.e. [244]Pu derived) in all of the Apollo 14 zircons requires that they were completely degassed of xenon after ~3900 Ma, or that the initial Pu/U ratio of the Moon was significantly different from the Earth's, which is unexpected in the current view of the Moon forming event. In conclusion, the xenon systematics in zircon are informative of multiple lunar surface processes including impact cratering, solar wind implantation, and high energy particle bombardment. Additionally, the relative behaviors of the U-Pb and U-Xe systems may make them ideal for investigating a range of terrestrial impact environments.

Declaration of Competing Interest

ACKNOWLEDGEMENTS

APPENDIX A. SUPPLEMENTARY MATERIAL

Supplementary data to this article can be found online at https://doi.org/10.1016/j.gca.2020.06.019.

REFERENCES

Baughman J. S. and Flowers R. M. (2018) Deciphering a 2 Gyr-long thermal history from a multichronometer (U-Th)/He study of the Phalaborwa Carbonate, Kaapvaal Craton, South Africa. *Geochem. Geophys. Geosyst.* **19**, 1581–1594.

Barboni M., Boehnke P., Keller B., Kohn I. E., Schoene B., Young E. D. and McKeegan K. D. (2017) Early formation of the Moon 4.51 billion years ago. *Sci. Adv.* **3**, e1602365.

Basford J. R., Dragon J. C., Pepin R. O., Coscio M. R. J. and Murthy V. R. (1973) Krypton and Xenon in lunar fines. In *Lunar Sci. Conf. IV*. Lunar and Plant. Ins., Houston, pp. 1915–1955 (abstr.).

Bateman H. (1910) Solution of a system of differential equations occurring in the theory of radioactive transformation. *Proc. Cambridge Philos. Soc. Math. Phys. Sci.* **15**, 423–427.

Boehnke P., Harrison T. M., Heizler M. T. and Warren P. H. (2016) A model for meteoritic and lunar [40]Ar/[39]Ar age spectra: addressing the conundrum of multi-activation energies. *Earth Planet. Sci. Let.* **453**, 267–275.

Brix M. R., Stöckhert B., Seidel E., Theye T., Thompson S. T. and Küster M. (2002) Thermobarometric data from a fossil zircon partial annealing zone in high pressure-low temperature rocks of eastern and central Crete, Greece. *Tectonophysics* **349**, 309–326.

Cassata W. S., Shuster D. L., Renne P. R. and Weiss B. P. (2010) Evidence for shock heating and constraints on Martian surface temperatures revealed by [40]Ar/[39]Ar thermochronometry of Martian meteorites. *Geochim. Cosmochim. Acta* **74**, 6900–6920.

Crow C. A. (2015) The Early Lunar Magmatic and Impact Histories Recorded by Apollo Zircons. University of California, Los Angeles, Thesis.

Crow C. A., Crowther S. A., Gilmour J. D., Busemann H., Moser D. E. and McKeegan K. D. (2015) U-Xe degassing ages of terrestrial and lunar impact zircons. *78th Meteor. Soc. Berkley, CA (abstr.)*.

Crow C. A., McKeegan K. D. and Moser D. E. (2017) Coordinated U-Pb geochronology, trace element, Ti-in-zircon thermometry and microstructural analysis of Apollo Zircons. *Geochim. Cosmochim. Acta* **202**, 264–284.

Crow C. A., Moser D. E. and McKeegan K. D. (2019) Shock metamorphic history of >4 Ga Apollo 14 and 15 zircons. *Meteorit. Planet. Sci.* **54**, 181–201.

Crowther S. A. and Gilmour J. D. (2013) The Genesis solar xenon composition and its relationship to planetary xenon signatures. *Geochim. Cosmochim. Acta* **123**, 17–34.

Crowther S. A., Mohapatra R. K., Turner G., Blagburn D. J., Kehm K. and Gilmour J. D. (2008) Characteristics and applications of RELAX, an ultrasensitive resonance ionization mass spectrometer for xenon. *J. Anal. Atomic Spec.* **23**, 921–1044.

Gaffney A. M., Borg L. E., Asmerom Y., Shearer C. K. and Burger P. V. (2011) Disturbance of isotope systematics during experimental shock and thermal metamorphism of a basalt with implications for Martian meteorite chronology. *Meteor. Planet. Sci.* **46**, 35–52.

Geyh M. A. and Schleicher H. (2012) Absolute Age Determination: Physical and Chemical Dating Methods and their Application. Springer Science & Business Media.

Gilmour J. D., Johnston W. A., Lyon I. C. and Turner G. (1992) RELAX-1, a refrigerator enhanced laser analyzer for xenon. *Meteoritics* **27**, 225 (abstr.).

Gilmour J. D., Lyon I. C., Johnston W. A. and Turner G. (1994) Relax - an ultrasensitive, resonance ionization mass-spectrometer for xenon. *Rev. Sci. Instru.* **65**, 617–625.

Gombosi D. J., Baldwin S. L., Watson E. B., Swindle T. D., Delano J. W. and Roberge W. G. (2015) Argon diffusion in Apollo 16 impact glass spherules: implications for [40]Ar-[39]Ar dating of lunar impact events. *Geochim. Cosmochim. Acta* **148**, 251–268.

Grange M. L., Pidgeon R. T., Nemchin A. A., Timms N. E. and Meyer C. (2013a) Interpreting U-Pb data from primary and secondary features in lunar zircon. *Geochim. Cosmochim. Acta* **101**, 112–132.

Grange M. L., Nemchin A. A. and Pidgeon R. T. (2013b) The effect of 1.9 and 1.4 Ga impact events on 4.3 Ga zircon and phosphate from an Apollo 15 melt breccia. *J. Geophys. Res. Planet.* **118**, 2180–2197.

Hayne P. O., Bandfield J. L., Seigler M. A., Vasavada A. R., Ghent R. R., Williams J.-P., Greenhagen B. T., Aharonson O., Elder C. M., Lucey P. G. and Paige D. A. (2017) Global regolith thermophysical properties of the moon from the diviner lunar radiometer experiment. *J. Geophys. Res.: Planets* **122**, 2371–2400.

Hohenberg C. M. and Rowe M. W. (1970) Spallation yields of xenon from irradiation of Cs, Ce, Nd, Dy, and a rare earth mixture with 730-mev protons. *J. Geophys. Res.* **75**, 4205–4209.

Hohenberg C. M., Hudson B., Kennedy B. M. and Podosek F. A. (1981) Xenon spallation systematics in Angra dos Reis. *Geochim. Cosmochim. Acta* **45**, 1909–1915.

Hopkins M. D. and Mojzsis S. J. (2015) A protracted timeline for lunar bombardment from mineral chemistry, Ti thermometry and U-Pb geochronology of Apollo 14 melt breccia zircons. *Contrib. Miner. Petrol.* **169**, 30.

Hörz F., Grieve R., Heiken G., Spudis P. and Binder A. (1991) Lunar surface processes. Cambridge University Press, Cambridge, England, p. 753.

Huang Ya.-H., Minton D. A., Zellner N. E. B., Hirabayashi M., Richardson J. E. and Fassett C. I. (2018) No change in recent lunar impact flux required based on modeling of impact glass spherule age distributions.k. *Geophys. Res. Let.* **45**, 6805–6813.

Hurst G. S., Payne M. G., Kramer S. D. and Young J. P. (1979) Resonance ionization spectroscopy and one-atom detection. *Rev. Mod. Phys.* **51**, 767–819.

Kaiser W. A. and Rajan R. S. (1973) The variation of cosmogenic Kr and Xe in a core from Estherville mesosiderite: direct evidence that the lunar 131Xe anomaly is a depth effect. *Earth Planet. Sci. Let.* **20**, 286–294.

Kamo S. L., Reimold W. U., Krogh T. E. and Colliston W. P. (1996) A 2.023 Ga age for the Vredefort impact event and a first report of shock metamorphosed zircons in pseudotachylitic breccias and granophyre. *Earth Planet. Sci. Let.* **144**, 369–387.

Kelly N. M., Flowers R. M., Metcalf J. R. and Mojzsis S. J. (2018) Late accretion to the Moon recorded in zircon (U-Th)/He thermochronometry. *Earth Planet. Sci. Let.* **482**, 222–235.

Lingenfelter R. E., Canfield E. H. and Hampel V. E. (1972) The lunar neutron flux revisited. *Earth Planet. Sci. Let.* **3**, 355–369.

Lugmair G. W. and Marti K. (1972) Neutron and spallation effects in fra mauro regolith. In *Lunar Sci. Conf. III.*. Lunar Planet. Inst., Houston, pp. 495–496 (abstr.).

Marti K., Lugmair G. W. and Urey H. C. (1970) Solar wind gasses, cosmic-ray spallation products and the irradiation history of Apollo 11 samples. In *Apollo 11 Lunar Sci. Conf. II*. Lunar Planet. Inst, Houston, pp. 1357–1367.

McKay D. S., Heiken G., Basu A., Blanford G., Simon S., Reedy R., French B. M. and Papike J. (1991) The Lunar Regolith. Cambridge University Press, Cambridge, England, p. 753.

Merrihue C. and Turner G. (1966) Potassium–argon dating by activation with fast neutrons. *J. Geophys. Res.* **71**, 2852–2857.

Merrihue C. M. (1965) Trace-element determinations and potassium–argon dating by mass spectroscopy of neutron-irradiated samples. *Trans. Am. Geophys. Union* **46**, 125.

Meshik A. P., Verchovsky A. B., Assonov S. S. and Shukolyukov Yu. A. (1987) New method of dating young uranium minerals. *Doklady Akademii Nauk USSR* **293**, 1476–1478.

Meyer C., Williams I. S. and Compston W. (1996) Uranium-lead ages for lunar zircons: evidence for a prolonged period of granophyre formation from 4.32 to 3.88 Ga. *Meteorit. Planet. Sci.* **387**, 370–387.

Morozova I., Shieh S. R., Moser D., Barker I. and Hanchar J. M. (2017) Strength and deformation of zircon at crustal and mantle pressures. John Wiley & Sons, Hoboken, New Jersey, pp. 167–182.

Moser D. E. (1997) Dating the schock wave and thermal imprint of the giant Vrederfort impact, South Africa. *Geology* **25**, 7–10.

Moser D. E., Flowers R. M. and Hart R. J. (2001) Birth of the Kaapvaal tectosphere 3.08 billion years ago. *Science* **291**, 465–468.

Moser D. E., Cupelli C. L., Barker I. R., Flowers R. M., Bowman J. R., Wooden J. and Hart J. R. (2011) New zircon shock phenomena and their use for dating and reconstruction of large imact structures revealed by electron nanobeam (EBSD, CL, EDS) and isotopic U-Pb and (U-Th)/He analysis of the Vredefort dome. *Can. J. Earth Sci.* **48**, 117–139.

Nemchin A. A., Whitehouse M. J., Pidgeon R. T. and Meyer C. (2006) Oxygen isotopic signature of 4.4-3.9 Ga zircons as a monitor of differentiation processes on the Moon. *Geochim. Cosmochim. Acta* **70**, 1864–1872.

Nemchin A. A., Pidgeon R. T., Whitehouse M. J., Vaughan J. P. and Meyer C. (2008) SIMS U-Pb study of zircon from Apollo 14 and 17 breccias: implications for the evolution of lunar KREEP. *Geochim. Cosmochim. Acta* **72**, 668–689.

Nemchin A. A., Timms N., Pidgeon R., Geisler T., Reddy S. and Meyer C. (2009) Timing of crystallization of the lunar magma ocean constrained by the oldest zircon. *Nat. Geosci.* **2**, 133–136.

Nemchin A. A., Grange M. L. and Pidgeon R. T. (2010) Distribution of rare earth elements in lunar zircon. *Am. Mineral.* **95**, 273–283.

Ozima M. and Podosek F. A. (2001) Noble Gas Geochemistry, second ed. Cambridge University Press, Cambridge, England, p. 302.

Payne M. G., Chen C. H., Hurst G. S. and Foltz G. W. (1981) Applications of resonance ionization spectroscopy in atomic and molecular physics. *Adv. At. Molecular Phys.* **17**, 229–274.

Pidgeon R. T., Nemchin A. A., van Bronswijk W., Geisler T., Meyer C., Compston W. and Williams I. S. (2007) Complex history of a zircon aggregate from lunar breccia 73235. *Geochim. Cosmochim. Acta* **71**, 1370–1381.

Podosek F. A. and Huneke J. C. (1971) Isotopic composition of ^{244}Pu fission xenon in meteorites: reevaluation using lunar spallation xenon systematics. *Earth Planet. Sci. Let.* **12**, 73–82.

Podosek F. A., Hunekee J. C., Burnett D. S. and Wasserburg G. J. (1971) Isotopic composition of xenon and krypton in the lunar soil and in the solar wind. *Earth Planet. Sci. Let.* **10**, 199–216.

Pravdivtseva O. and Shukolyukov Yu. (1994) The modeling of xenon and lead isotopes migration in zircon and in pitchblende under hydrothermal conditions. In *ICOG 8, Berkeley, CA, June 5–11*, p. 256.

Ragettli R. A., Hebeda E. H., Singer P. and Wieler R. (1994) Uranium-Xenon chronology: precise determination of λsf* 136Ysf for spontaneous fission of 238U. *Earth Planet. Sci. Let.* **128**, 653–670.

Reimold W. U., Meshik A. P., Smits G., Pravdivtseva O. V. and Shukolyukov Y. A. (1995) Fission xenon dating of witwatersrand uraninites: implications for geological activity in the central kaapvaal craton about 1 Ga ago. *Geochim. Cosmochim. Acta* **59**, 5177–5190.

Reimold W. U. and Gibson R. L. (1996) Geology and evolution of the Vrederfort impact structure, South Africa. *J. African Earth Sci.* **23**, 125–162.

Reimold W. U., Pybus G. Q. J., Kruger F. J., Layer P. W. and Koeberl C. (2000) The Anna's rust sheet and related gabbroic intrusions in the Vredefort dome-kibaran magmatic event on the Kaapvaal craton and beyond? *J. African Earth Sci.* **31**, 499–521.

Reedy R. C. and Arnold J. R. (1972) Interactions of solar and galactic cosmic-ray particles with the Moon. *J. Geophys. Res.* **77**, 537–555.

Shukolyukov J., Kristen T. and Jesserberger E. K. (1974) The Xe-Xe spectrum technique, a new dating method. *Earth Planet. Sci. Let.* **24**, 271–281.

Shukolyukov Yu. A., Kapusta Ya S., Verchovsky A. B., Verkhovskij A. B., Vaajoki M. and Vaas'oki M. (1979) Neutron-induced fission xenon dating of zircon. *Geochem. Int.* **16**, 122–133.

Shukolyukov Yu. A., Fugzan M. M., Paderin I. P., Sergeev S. A. and Krylov D. P. (2009) Unusually high thermal stability of the uranium-xenon isotopic system in nonmetamict zircons. *Dokl. Earth Sci.* **425**, 287–290.

Shuster D. L. and Cassata W. S. (2015) Plaeotemperatures at the lunar surfaces from open system behavior of cosmogenic ^{38}Ar and radiogenic ^{40}Ar. *Geochim. Cosmochim. Acta* **155**, 154–171.

Spray J. G. (1995) Pseudotachylyte controversy: fact or fiction? *Geology* **23**, 1119–1122.

Taylor D. J., McKeegan K. D. and Harrison T. M. (2009) Lu–Hf zircon evidence for rapid lunar differentiation. *Earth Planet. Sci. Lett.* **279**, 157–164.

Teitsma A. and Clarke W. B. (1978) Fission xenon dating. *J. Geophys. Res.* **83**, 5443–5453.

Teitsma A., Clarke W. B. and Allegre C. J. (1975) Spontaneous fission-neutron fission xenon. A new technique for dating geological events. *Science* **189**, 878–880.

Timms N. E., Reddy S. M., Healy D., Nemchin A. A., Grange M. L., Pidgeon R. T. and Hart R. (2012) Resolution of impact related microstructures in lunar zircon: a shock-deformation mechanism map. *Meteorit. Planet. Sci.* **47**, 120–141.

Timms N. E., Erickson T. M., Pearce M. A., Cavosie A. J., Tohver E., Reddy S. M., Zanetti M. R., Nemchin A. A. and Wittmann A. (2017) A pressure-temperature phase diagram for zircon at extreme conditions. *Earth Sci. Rev.* **165**, 185–202.

Turner G., Huneke J. C., Podosek F. A. and Wasserburg G. J. (1971) ^{40}Ar-^{39}Ar ages and cosmic ray exposure ages of Apollo 14 samples. *Earth Planet. Sci. Let.* **12**, 19–35.

Turner G., Busfeld A., Crowther S. A., Harrison M., Mojzsis S. J. and Gilmour J. (2007) Pu-Xe, U-Xe, U-Pb chronology and isotopc systematics of ancient zircons from Western Australia. *Earth Planet. Sci. Let.* **261**, 491–499.

Turner G. (2008) Neutron exposure on the lunar surface based on ^{235}U fission in zircon. *71st Annual Meteoritical Society Meeting* (abstr.).

Weber W. J. (1990) Radiation-induced defects and amorphization in zircon. *J. Mater. Res.* **5**, 2687–2697.

Weber W. J., Ewing R. C. and Wang L.-M. (1994) The radiation-induced crystalline to amorphous transition in zircon. *J. Mater. Res.* **9**, 688–698.

Wielicki M. M., Harrison T. M. and Schmitt A. K. (2012) Geochemical signatures and magmatic stability of terrestrial impact produced zircon. *Earth Planet. Sci. Let.* **321–322**, 20–31.

Woolum D. S. and Burnett D. S. (1974) In-situ measurement of the rate of ^{235}U fission induced by lunar neutrons. *Earth Planet. Sci. Let.* **21**, 153–163.

Zellner N. E. B., Delano J. W., Swindle T. D., Barra F., Olsen E. and Whittet D. C. B. (2009) Evidence from 40Ar/39Ar ages of lunar impact glasses for an increase in impact rate ∼800 Ma ago. *Geochim. Cosmochim. Acta* **73**, 4590–4597.

Associate editor: Gregory F. Herzog